Available online at www.sciencedirect.com
ScienceDirect
Biochimica et Biophysica Acta 1777 (2008) 84–93
Biochimica et Biophysica Acta
BBA
www.elsevier.com/locate/bbabio

A structural investigation of complex I and I+III_2 supercomplex from *Zea mays* at 11–13 Å resolution: Assignment of the carbonic anhydrase domain and evidence for structural heterogeneity within complex I

Katrin Peters [a], Natalya V. Dudkina [b], Lothar Jänsch [c], Hans-Peter Braun [a,*], Egbert J. Boekema [b]

[a] *Institute for Plant Genetics, Faculty of Natural Sciences, Leibniz Universität Hannover, Herrenhäuser Str. 2, D-30419 Hannover, Germany*
[b] *Groningen Biomolecular Sciences and Biotechnology Institute, University of Groningen, Nijenborgh 4, 9747 AG Groningen, The Netherlands*
[c] *Proteome Research Group, Division of Cell and Immune Biology, Helmholtz Centre for Infection Research, Inhoffenstraße 7, D-38124 Braunschweig, Germany*

Received 21 August 2007; received in revised form 18 October 2007; accepted 19 October 2007
Available online 4 November 2007

Abstract

The projection structures of complex I and the I+III_2 supercomplex from the C_4 plant *Zea mays* were determined by electron microscopy and single particle image analysis to a resolution of up to 11 Å. Maize complex I has a typical L-shape. Additionally, it has a large hydrophilic extra-domain attached to the centre of the membrane arm on its matrix-exposed side, which previously was described for *Arabidopsis* and which was reported to include carbonic anhydrase subunits. A comparison with the X-ray structure of homotrimeric γ-carbonic anhydrase from the archaebacterium *Methanosarcina thermophila* indicates that this domain is also composed of a trimer. Mass spectrometry analyses allowed to identify two different carbonic anhydrase isoforms, suggesting that the γ-carbonic anhydrase domain of maize complex I most likely is a heterotrimer. Statistical analysis indicates that the maize complex I structure is heterogeneous: a less-abundant "type II" particle has a 15 Å shorter membrane arm and an additional small protrusion on the intermembrane-side of the membrane arm if compared to the more abundant "type I" particle. The I+III_2 supercomplex was found to be a rigid structure which did not break down into subcomplexes at the interface between the hydrophilic and the hydrophobic arms of complex I. The complex I moiety of the supercomplex appears to be only of "type I". This would mean that the "type II" particles are not involved in the supercomplex formation and, hence, could have a different physiological role.

Keywords: Complex I; Cytochrome *c* reductase; Carbonic anhydrase; Supercomplex; Electron microscopy, *Zea mays*

1. Introduction

Complex I is the major entrance point of electrons to the respiratory chain. It catalyses the transfer of two electrons from NADH to quinone, which is coupled to the translocation of four protons across the inner mitochondrial membrane [1–3]. The subunit composition of complex I is highly variable depending on the type of organism. Bovine and human complex I are composed of about 46 different subunits and have a molecular weight of about 1 MDa. Complex I of prokaryotes and chloroplasts are substantially smaller and composed mostly of 14 subunits that are homologues of a "core" complex of mitochondrial complex I. They have been defined as the "minimal" enzyme. The remaining subunits are so-called "accessory" subunits [3]. Complex I consists of a hydrophobic membrane arm and a hydrophilic peripheral arm, which protrudes into the matrix. Together they give complex I an unique L-shape, as has been revealed at low-resolution by three-dimensional electron microscopy [4–6]. The crystal structure of the peripheral arm of complex I from *Thermus thermophilus* has been solved [7]. The positions of eight subunits and all redox centres of the enzyme were determined, including nine iron–sulfur centres.

The main known function of the membrane arm is proton translocation [8], but the precise functions of the membrane domain are not well understood because of a lack of high-resolution structural data. However, a medium-resolution projection map at 8 Å of complex I from *E. coli* was recently obtained by electron microscopy [9]. It indicates the presence of about 60 transmembrane α-helices, both perpendicular to the

* Corresponding author. Tel.: +49 511 7622674; fax: +49 511 7623608.
E-mail address: braun@genetik.uni-hannover.de (H.-P. Braun).

0005-2728/$ - see front matter © 2007 Elsevier B.V. All rights reserved.
doi:10.1016/j.bbabio.2007.10.012

membrane plane and tilted, which is consistent with secondary structure predictions. A possible binding site and access channel for quinone is found at the interface with the peripheral arm. Tentative assignment of individual subunits to the features of the map has been made. The NuoL and NuoM subunits, which were proposed to be responsible for proton translocation, are localized at the tip of the membrane arm of complex I. Since this tip is at a substantial distance to the redox centres of the peripheral arm of complex I, conformational changes most likely play a role in the coupling between electron transfer and proton pumping.

Complex I can form stable associations with complex III of the respiratory chain [10,11]. This interaction is especially stable in plants. An investigation by EM and single particle analysis revealed a lateral association of dimeric complex III to the tip of the membrane part of complex I in *Arabidopsis* [12]. The functional role of the $I+III_2$ supercomplex so far is unknown.

Complex I of plant mitochondria resembles complex I of other multicellular organisms but includes some extra subunits [13–15]. As a consequence, its overall molecular mass is slightly larger than that of complex I of beef [16]. Some of the extra subunits introduce side-activities into plant complex I. In probably all higher eukaryotes, the "acyl carrier protein" of the mitochondrial fatty acid biosynthesis pathway is integrated into complex I [17,18]. However, occurrence of this protein in complex I of plants recently has been disputed [19]. Additionally, L-galactono-1,4-lactone dehydrogenase (GalLDH), the terminal enzyme of the mitochondrial ascorbate biosynthesis pathway, forms part of complex I in plants [20]. Furthermore, plant mitochondria include a group of five structurally similar 30 kDa proteins which resemble a γ-type carbonic anhydrase of the archaebacterium *Methanosarcina thermophila*. A structural characterization by single particle electron microscopy of complex I from *Arabidopsis* and the green alga *Polytomella* indicated a plant-specific spherical extra-domain of about 60 Å in diameter, which is attached to the central part of the membrane arm of complex I on its matrix face [15]. This spherical domain is proposed to be composed of the γ-carbonic anhydrase subunits. Although the inner features of the domain could not be resolved it is probably arranged as a trimer of three subunits, because γ-carbonic anhydrase of *Methanosarcina thermophila* is known to have a trimeric structure [21,22].

The functional role of the complex I integrated carbonic anhydrases in plants is not quite understood. It was speculated that they form part of an active CO_2 transport system between mitochondria and chloroplasts for efficient CO_2 fixation during photosynthesis [23]. CO_2, one of the main substrates of photosynthesis, is often growth limiting in plants. The CO_2 concentration within chloroplasts especially declines if plants are grown in the presence of high-light conditions, enabling high rates of CO_2 fixation. Furthermore, the CO_2 concentration declines at high temperature due to Ribulose-1,5-bisphosphate Carboxylase/Oxygenase (RubisCO) kinetics and water solubility of oxygen and CO_2. As a consequence, the Oxygenase side-activity of RubisCO increases dramatically, giving rise to the formation of phosphoglycolate. This compound cannot be used for the Calvin cycle and is recycled by the so-called "photorespiration" pathway. Finally, during photorespiration, large amounts of CO_2 are liberated in the mitochondria. In summary, CO_2 concentration in the chloroplasts of plant cells often is low. At the same time, the mitochondria produce large amounts of CO_2. Rapid conversion of mitochondrial CO_2 into bicarbonate by carbonic anhydrases is speculated to form the basis of an active indirect CO_2 transport mechanism between mitochondria and chloroplasts. Indeed, genes encoding the complex I integrated carbonic anhydrases are down-regulated in *Arabidopsis*, if plants are cultivated in the presence of elevated CO_2 concentration [22]. An analogous role of complex I was reported in the context of a cyanobacterial CO_2 concentrating mechanism [24].

A characterization of maize (*Zea mays*) complex I was initiated to further investigate the physiological role of the mitochondrial carbonic anhydrases in plants. In contrast to the "C_3" plant *Arabidopsis*, maize is a so-called "C_4" plant that uses phosphoenolpyruvate (PEP) for pre-fixation of CO_2 in the form of a four-carbon (C_4) compound. Pre-fixation is carried out in specialized cells termed mesophyll cells, which also carry out the photosynthetic light reactions and water splitting. The final CO_2 fixation by RubisCO takes place in so-called bundle sheath cells, which do not carry out photosynthetic water splitting. C_4 metabolism is based on the transfer of C_4-compounds from mesophyll to bundle sheath cells and liberation of CO_2 in bundle sheath cells. As a consequence, the final CO_2 fixation by RubisCO is very efficient and photorespiration is avoided. Therefore, the functional role of the mitochondrial carbonic anhydrases might differ between *Arabidopsis* and maize. However, in certain subtypes of C_4 metabolism, which use a mitochondrial enzyme for CO_2 release in bundle sheath cells, the presence of carbonic anhydrases in mitochondria might be especially important.

Here, we describe a structural analysis by single particle electron microscopy of maize complex I. It has the same L-shaped form like *Arabidopsis* complex I, including the extra carbonic anhydrase domain. This domain is, as well as other features, much better resolved in the current projection maps, and comparison to the high-resolution X-ray structure of the γ-carbonic anhydrase now shows it to be a trimer. Mass spectrometry was performed to evaluate the composition of the carbonic anhydrase trimer. In addition, the structure of the respiratory $I+III_2$ supercomplex was analyzed. This supercomplex has a horse-shoe structure, identical to the one found in *Arabidopsis*. It appears to be a very stable, rigid structure that allowed the determination of projection maps at 12 Å resolution. New insights into the complex I–complex III interaction are presented.

2. Materials and methods

2.1. Cultivation of maize seedlings

Green maize seedlings (*Zea mays convar saccharata* L. "Tasty Sweet" F1) were cultivated in a greenhouse under long-day conditions (16 h light, 8 h dark) at 22 °C for 9 days. Etiolated maize seedlings were cultivated in growth chambers in the absence of light at 22 °C for the same time period.

2.2. Isolation of maize mitochondria

Starting material for organelle preparations were 100 g of green and etiolated tissue. The material was suspended each in 500 ml of ice-cold "grinding buffer" (0.4 M mannitol, 1.0 mM EGTA, 25.0 mM MOPS, 0.1% [w/v] bovine serum

albumin [BSA], 15 mM β-mercaptoethanol, and 0.05 mM phenylmethylsulfonyl fluoride [PMSF]/KOH, pH 7.8). The cells were disrupted by homogenization for three periods of 10 s using a Waring blender and then filtered through two layers of muslin. Mitochondria were isolated by differential centrifugation and Percoll density gradient centrifugation as described by Braun et al. [25]. The three-step Percoll gradients for density gradient centrifugation contained 14%, 26%, and 45% Percoll in 0.8 M mannitol, 2.0 mM EGTA, 20.0 mM KH_2PO_4/KOH, pH 7.2. After gradient centrifugation (45 min at 70,000 ×*g*), mitochondria were isolated from the 26%/45% interphase. To remove the Percoll the purified mitochondria were centrifuged three times in "resuspension buffer" (0.4 M mannitol, 1.0 mM EGTA, 10.0 mM KH_2PO_4, 0.2 mM PMSF/KOH, pH 7.2) for 10 min at 14,500 ×*g*.

Purities of our organelle preparations were investigated by analyses of protein complex compositions using 2D Blue-native/SDS-PAGE (see below) [26]. Mitochondrial fractions included all the known protein complexes of the OXPHOS system but were devoid of plastidic complexes, e.g. the photosystems, the b_6f complex and the plastidic ATP synthase complex. The latter two complexes are also formed in etioplasts but were absent in mitochondrial fractions isolated form maize seedlings cultivated in the dark (data not shown). Furthermore, the subunit completeness of all OXPHOS complexes was very good indicating that the purified organelles were isolated in a very intact form.

2.3. Gel electrophoreses procedures and immunoblotting

One-dimensional Blue-native PAGE and two-dimensional Blue-native/SDS-PAGE were carried out as outlined in Heinemeyer et al. [27]. Proteins were either visualized by Coomassie blue colloidal staining [28] or blotted onto nitrocellulose filters. Blots were incubated over night with an antiserum directed against the C-terminal half of a complex I integrated carbonic anhydrase of *Arabidopsis* (encoded by locus At1g47260; [22]). Visualization of immune-positive protein spots was performed using biotinylated secondary antibodies, avidin, and horseradish peroxidase (Vectastain ABC kit, Vector laboratories, Burlingame, CA, USA).

2.4. Protein analyses by mass spectrometry

Proteins of interest were cut out of 2D Blue-native/SDS gels and pre-treated for mass spectrometry (MS) analyses as described previously in Eubel et al. [11]. Selected tryptic peptides were sequenced by Electrospray Ionization MS/MS using the Q-TOF II mass spectrometer (Micromass, Watres, Milford, MA, USA). Proteins were identified by MASCOT (http://www.matrixscience.com/) using the NCBI protein database.

2.5. Purification of complex I and I+III$_2$ supercomplex from maize by sucrose gradient ultracentrifugation

Isolated mitochondria were solubilized by digitonin (5 mg of detergent per mg of mitochondrial protein), and protein complexes were subsequently resolved by sucrose gradient ultracentrifugation as previously described by Dudkina et al. [12]. Fractions were removed from the gradient from bottom to top. Protein complexes present in individual fractions were resolved by BN PAGE and identified on the basis of their subunit compositions on second gel dimensions, which were carried out in the presence of SDS [14]. Fractions including complex I and the I+III$_2$ supercomplex were directly used for EM analysis.

2.6. Electron microscopy and single particle analysis

Selected fractions of the sucrose gradient including the I+III$_2$ supercomplex and complex I were directly used for electron microscopy. Electron microscopy was performed on a Philips CM12 electron microscope equipped with a slow-scan CCD camera. Data acquisition and single particle analyses including alignments of projections with multi-reference and non-reference procedures, multivariate statistical analysis and classification, was carried out as outlined by Dudkina et al. [12]. Resolution was determined according to Van Heel 1987 [29] by 2σ and 3σ criteria.

The trimeric X-ray structure of γ-carbonic anhydrase (PDB accession number 1QRE) from *Methanosarcina thermophila* [30] and the hydrophilic domain of complex I (PDB accession number 2FUG) from *Thermus thermophilus* [7] were used to model the carbonic anhydrase domain and the hydrophilic arm of complex I. VIS5D software (http://www.ssec.wisc.edu/~billh/vis5d.html) and PyMOL software were used for visualization. For the modeling of the I+III$_2$ supercomplex we used the X-ray structures of cytochrome bc_1 complex (PDB accession number 1BGY) from bovine mitochondria [31] and 3D EM model of complex I from *Yarrowia lipolytica* [6].

3. Results

3.1. Characterization of complex I and the I+III$_2$ supercomplex of maize

Mitochondria from green and etiolated maize seedlings were purified to investigate the structure of complex I and the I+III$_2$

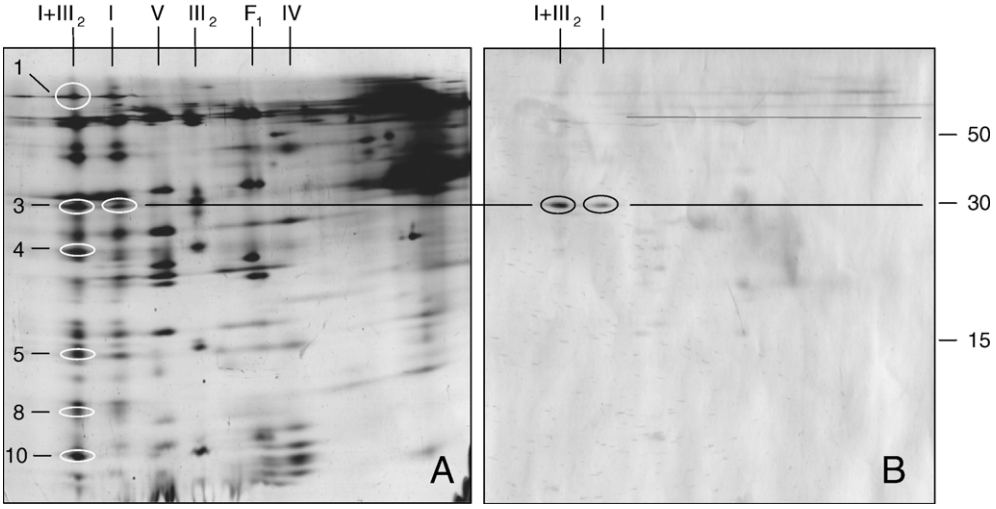

Fig. 1. Two-dimensional resolution of mitochondrial proteins from etiolated maize seedlings by Blue-native/SDS-PAGE. (A) Silver-stained gel. (B) Immunological detection of carbonic anhydrase on a corresponding Western blot. The identities of the resolved protein complexes and supercomplexes are given above the gel and the blot, the molecular masses of standard proteins to the right of the blot (in kDa). Proteins subjected to analyses by mass spectrometry are circled on the gel and numbered consecutively (for results see Table 1).

supercomplex from a C_4 plant. The OXPHOS system of maize was analyzed by 2D Blue-native/SDS-PAGE. On the first gel dimension, complex I runs at about 1000 kDa and the $I+III_2$ supercomplex at 1500 kDa (data not shown). Subunits of the OXPHOS complexes were resolved by SDS-PAGE. The subunit compositions of the OXPHOS complexes of mitochondria of etiolated maize seedlings (Fig. 1) resemble the ones of *Arabidopsis* [14]. On the 2D gel, complex III_2 is resolved into 9 distinct subunits, complex I into >25 and the $I+III_2$ supercomplex also into >25 subunits. The latter two complexes probably include several further subunits, which are invisible on the 2D gels due to overlapping positions. The subunit composition of complex I and the $I+III_2$ supercomplex of mitochondria of green maize seedlings was indistinguishable from the ones obtained for etiolated seedlings upon analyses by 2D Blue-native PAGE (data not shown).

The presence of carbonic anhydrases within complex I and the $I+III_2$ supercomplex of maize was investigated by immunoblotting using an antibody directed against a complex I integrated carbonic anhydrase of *Arabidopsis*. The antibody specifically recognizes an epitope on a protein in the 30 kDa range of both complexes (Fig. 1B). The presence of carbonic anhydrases within complex I and the $I+III_2$ supercomplex of maize was confirmed by mass spectrometry (MS). For this approach, the 30 kDa spot and 5 further spots of the $I+III_2$ supercomplex were cut out from a 2D BN/SDS gel, trypsinated and prepared for MS analysis. Overall, 13 peptides sequences were obtained (Table 1), which exactly match peptide sequences encoded by the rice genome (the complete genome sequence of maize currently is not available; rice is the closest relative of maize to be completely sequenced). The peptides are part of 8 different proteins, four of which belong to complex I (75, 23 and 11 kDa subunits and a protein homologous to a complex I integrated carbonic anhydrase of rice), and four of which belong to complex III_2 (cytochrome c_1, the Rieske iron–sulfur protein, 14 kDa and 8.2 kDa subunits). Sequence identities between the maize peptides and the corresponding amino acid sequences from *Arabidopsis* are in the range of 65 to 90% (data not shown).

For EM analyses, purified mitochondrial fractions from green and etiolated seedlings were loaded onto sucrose gradients and protein complexes were separated by ultracentrifugation. Afterwards, gradients were fractionated and small aliquots of all fractions were analysed by 1D Blue-native PAGE to monitor the protein complex composition of the fractions (Fig. 2). Fractions close to the bottom of the gradients included pure complex I and $I+III_2$ supercomplex. These fractions were selected for further analyses using single particle EM.

3.2. Electron microscopy

Negatively stained electron microscopy specimens of fractions 3 and 4 for the green seedlings and fractions 4 and 5 for the etiolated seedlings indicated large numbers of projections of complex I and $I+III_2$ supercomplex suitable for single particle image analysis. We analyzed a selected data set of about 28,000 projections from green maize, which was grown in the light, and a data set of about 12,000 projections from etiolated maize, which was grown in the dark. An initial analysis by multi-reference alignment, multivariate statistical analysis and classification of the projections indicated that both sets comprised the same classes of projections with similar numbers of particles. Hence, the two data sets were also combined in one large data set and analysed together, to get better resolution in the final projection maps.

After classification of the separate data sets and combined set of projections, a gallery of different projection maps of singular complex I and the $I+III_2$ supercomplex was obtained (Fig. 3). The $I+III_2$ supercomplex has one preferable orientation in a specific top-view position (Fig. 3A). Only 75 views could be assigned to side view positions; the sum of the best 32 projections is shown in Fig. 3B. Due to the very low numbers of particles, the resolution of this side view projection is very limited. The classes shown in parts D–K of Fig. 3 represent side views of complex I. All these projections show the membrane-embedded arm in horizontal position and the hydrophilic arm in about vertical position. The classes D/H and G/I represent

Table 1

Spot no.[a] (peptide)	Identified peptide sequence[b]	Protein identity[c]	Accession no.[d] (organism)
1 (b)	GSGEEIGTYVEK	75 kDa subunit, complex I	gi|115454943 (rice)
(c)	SNYLMNTSIAGLEK	75 kDa subunit, complex I	gi|125545494 (rice)
3 (b)	LGSTIQGGLR	Carbonic anhydrase, complex I	gi|115473681 (rice)
(c)	IPSGEVWVGNPAK	Carbonic anhydrase, complex I	gi|115473681 (rice)
(d)	DLVGVAYTEEETK	cyt c1, complex III	gi|115442085 (rice)
(f)	DVVSFLSWAAEPEMEER	cyt c1, complex III	gi|34907202 (rice)
4 (b)	LANSVDVASLR	Rieske iron-sulfur protein, complex III	P49727 (maize)
(c)	NVTINYPFEK	23 kDa TYKY subunit, complex I	gi|115455639 (rice)
(d)	SINTLFLTEMVR	23 kDa TYKY subunit, complex I	gi|115455639 (rice)
(e)	NQDAGLADLPATVAAVK	Rieske iron-sulfur protein, complex III	P49727 (maize)
5 (b)	QSLGALPLYQR	14 kDa protein, complex III	gi|115471095 (rice)
8 (b)	GFVMEFAENLILR	11 kDa subunit of complex I (At1g67350)	gi|115454659 (rice)
10 (b)	AVVYAISPFQQK	8.2 kDa protein, complex III	gi|115466706 (rice)

[a] The spot numbers correspond to the numbers given on Fig. 1.
[b] Peptides were identified by ESI-MS/MS as outlined in the Material and methods section.
[c] Proteins were identified by MASCOT (http://www.matrixscience.com/) using the NCBI protein database.
[d] NCBI protein accession codes of the most similar annotated proteins.

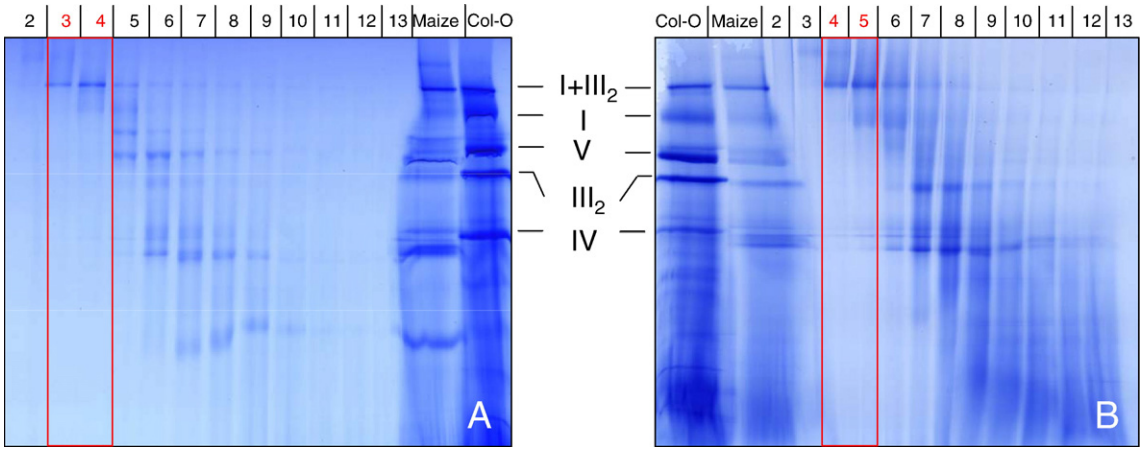

Fig. 2. Documentation of the purification of complex I and the I+III_2 supercomplex from maize by 1D Blue-native PAGE. Mitochondrial fractions from green (A) and etiolated (B) maize seedlings were solubilized using 5% digitonin and protein complexes were separated by sucrose gradient ultracentrifugation as outlined in the Materials and methods section. Gradients were fractionated into 13 fractions from bottom to top and resolved by Blue-native PAGE. As a control, digitonin solubilized total mitochondrial proteins from maize and *Arabidopsis* (Col-O) were directly resolved on the 1D Blue-native gels. Identities of the resolved protein complexes are given between the gels. Fractions 3 and 4 for the green seedlings and fractions 4 and 5 for the etiolated seedlings were used for EM analyses (Figs. 3 and 4).

identical particles which differ in their handedness caused by a different orientation on the carbon support film. There are small numbers of particles which have a shorter peripheral arm caused by the absence of the NADH-oxidizing domain (classes G, I). About 600 projections could be assigned to a top view of complex I (Fig. 3C). In this view the membrane arm is bent, as previously reported for *Arabidopsis* and *Polytomella* complex I [12,15]. The density at the left of the bend membrane arm of complex I probably represents the projected subunits of the peripheral arm. The panels J and K of Fig. 3 demonstrate identical structures of complex I from green and etiolated maize, respectively. This is in line with the identical subunit compositions obtained for complex I of etiolated and green maize seedlings upon analysis by 2D Blue-native PAGE. The best projection map of the I+III_2 supercomplex (Fig. 3A) has a resolution of 12 Å, the best one of complex I (Fig. 3D) has a resolution of 11 Å, both with the 2σ criterion [29].

Careful analyses of the classification results revealed the presence of two types of complex I particles in maize, which were designated type I and type II. The length of the membrane arm of the type I (Fig. 3D) is about 230 Å (including detergent), which is similar to the one of complex I from *Arabidopsis* [12], while the membrane arm of type II (Fig. 3E) has a length of 215 Å. Furthermore, the membrane arm of the type II complex I exhibits some extra density on its intermembrane-space exposed side (Fig. 3, marked by a white arrow). Another micro-variation concerns the angle between the hydrophobic membrane arm and the hydrophilic peripheral arm, which in most particles is 115° but in a small subset of particles is 125° (Fig. 3F). This variation only was observed for type I complex I. It is not clear if this is a matter of a different orientation of complex I on the carbon support film, intrinsic flexibility or a real structural difference.

The presence of two different structural classes of complex I from maize prompted us to re-analyze the complex I structure of *Arabidopsis*. Complex I was isolated from non-green suspension cell cultures as described before [12] but additionally from green *Arabidopsis* plants. Structural analysis of 10,000 projections from the cell culture and 13,500 from green plants did not reveal significant differences in complex I structures (not shown). Therefore, the two data sets were combined to calculate an average projection of most optimal resolution (Fig. 3L). The structure of complex I from *Arabidopsis* very much resembles the type I structure of complex I from maize (Fig. 3D).

Maize complex I comprises the plant-specific carbonic anhydrase domain which previously was reported for *Arabidopsis* [12] and *Polytomella* [15]. This spherical extra-domain has a diameter of about 60 Å (marked by white arrowheads in Fig. 3). Furthermore, in comparison to other organisms, a small intermembrane-space-exposed protrusion of unknown function is attached to the membrane arm of complex I from *Arabidopsis*, *Polytomella* and maize (marked by black arrows in Fig. 3).

We were able to reach a resolution of 11 Å for a complex I projection map from maize. This allows us to compare it with the X-ray structure of trimeric carbonic anhydrase from *Methanosarcina thermophila* [30], the only known X-ray structure of a γ-type carbonic anhydrase (Fig. 4A, B). The truncated X-ray structure has a rather similar overall shape and a size of approximately 60 Å, and nicely fits to the matrix-exposed extra-domain of the side view projection of maize complex I (Fig. 4A). The fit appears to give a good match between the truncated carbonic anhydrase model and the EM data. For instance, a prominent groove running from the upper left to the middle right position in the truncated carbonic anhydrase model is also visible in the EM projection maps as a negative stain-filled region in the same position (Fig. 4A). We also tried to assign the position of the carbonic anhydrase on the top view of the I+III_2 supercomplex by comparison with the side view and the most likely position is presented in Fig. 4B.

In order to assign the positions of complex I and complex III_2 within the I+III_2 supercomplex we used the X-ray structures of cytochrome *c* reductase from beef [31], the peripheral arm of complex I from *Thermus thermophilus* [7] and a low-resolution

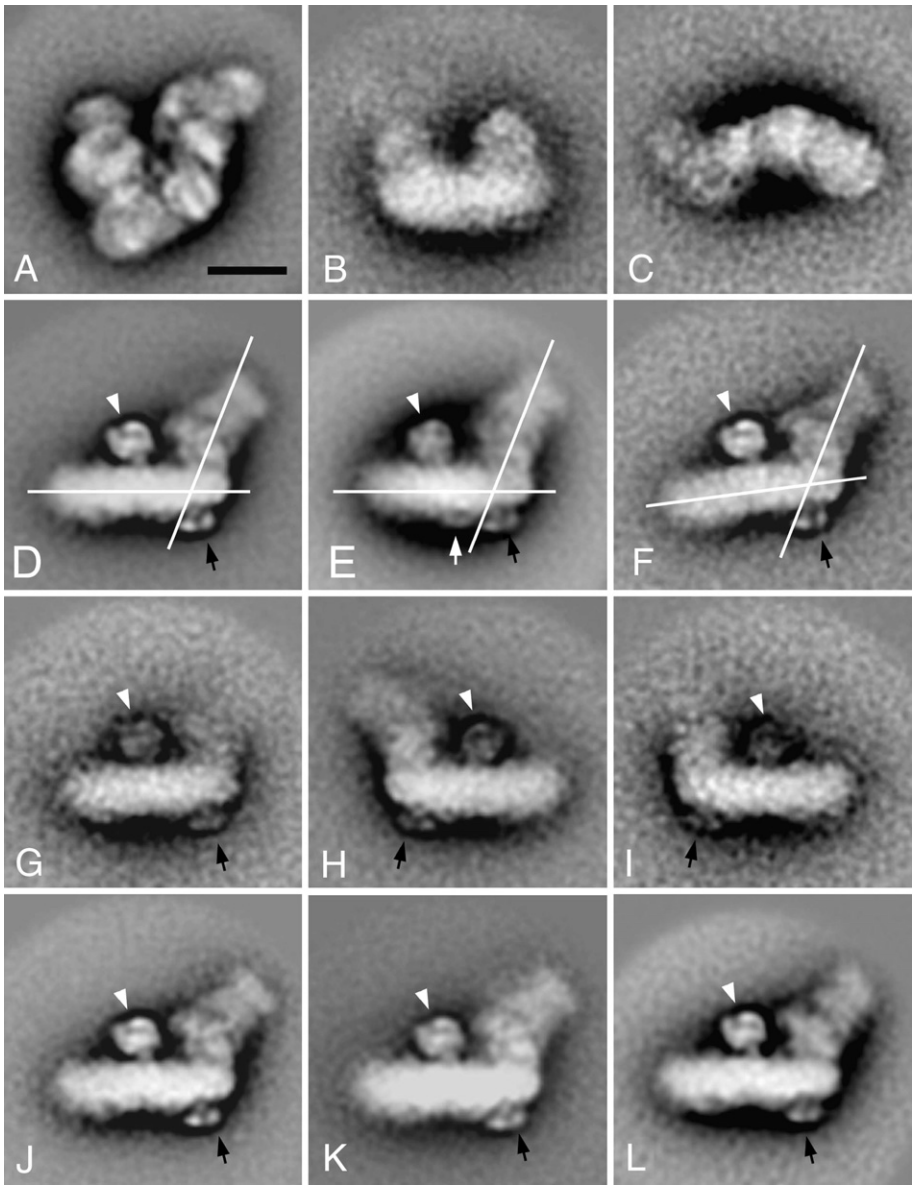

Fig. 3. Gallery of complex I and I+III$_2$ supercomplex projection maps from *Zea mays*. A: Average of 1024 projections of the I+III$_2$ supercomplex (top-view). B: Average of 32 projections of the I+III$_2$ supercomplex (side view). C: Average of 512 projections representing a top-view of complex I. D–K: average side view projection maps of complex I in different orientations. D: average of 4096 projections of the most prominent form of side view particles (type I), E: average of 1024 projections of a minor form of complex I (type II), F: average of 512 projections of another minor form of complex I with an altered angle between the membrane and the peripheral arm (type I), G: average of 512 projections of complex I particles lacking the NADH-oxidizing domain, H: average of 1024 projections of type I complex I in an orientation opposite to the one shown in D, I: average of 512 projections of complex I particles lacking the NADH-oxidizing domain in an orientation opposite to the one shown in G, J: type I complex I particles from green maize plants (average of 1024 projections), K: type I complex I particles from etiolated maize plants (average of 1024 projections). L: Average of 4096 projections of complex I from *Arabidopsis thaliana*. The white arrowhead marks the carbonic anhydrase domain of complex I and the black arrow another plant-specific domain localized on the intermembrane-space exposed side of the membrane arm of complex I. The white arrow indicates an extra density on the intermembrane-space exposed side of type II complex I particles.

3D EM model of *Yarrowia lipolytica* [6] to do a manual fitting in the *Zea mays* EM projections (Fig. 4). For each of the components there is only one possible way to obtain a good fit, which means that the components match the EM maps within the positions indicated, although small rotational displacements (up to 10°) would still be possible. The fittings indicate that the top-view map of the supercomplex cannot be precisely parallel to the membrane plane because the projected structure of complex III$_2$ does not show the expected two-fold rotational symmetry, as it would do without any tilt away from the membrane view (Fig. 4C). As a consequence, formation of this supercomplex possibly causes a slight bend of the inner membrane which previously was reported for the dimeric ATP synthase supercomplex of yeast and *Polytomella* [32]. However, the side view of the I+III$_2$ supercomplex (Fig. 4D) rather indicates a parallel position of the long axes of the peripheral complex I arm and complex III$_2$ with respect to the inner membrane. Therefore, the precise orientation of complexes I and III$_2$ within

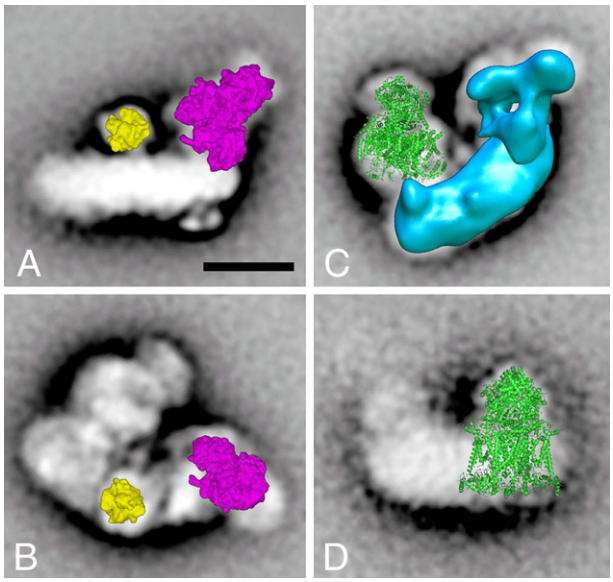

Fig. 4. Fitting of 3D structures of complex I, complex III_2, and trimeric γ-carbonic anhydrase from various sources to the single particle structures of the maize $I+III_2$ supercomplex and maize complex I. Fittings were carried out using truncated versions at 10 Å of the atomic structures of trimeric γ-carbonic anhydrase from *Methanosarcina thermophila* [28], the peripheral arm of complex I from *Thermus thermophilus* [7], the 3D EM structure of complex I from *Yarrowia lipolytica* (blue) [6] and the X-ray structure of complex III_2 from beef [29]. (A) Assignment of trimeric carbonic anhydrase (yellow) and the peripheral arm of complex I (purple) on maize complex I in side view position. (B) Assignment of the same structures on a top-view of the maize $I+III_2$ supercomplex. (C) Assignment of the complex I (blue) and complex III_2 (green) structures on the maize $I+III_2$ supercomplex in top-view position. (D) Assignment of the same structures on a side view of the maize $I+III_2$ supercomplex. The bar equals 100 Å.

the $I+III_2$ supercomplex currently still has to be taken with caution.

4. Discussion

The investigation of complex I and the $I+III_2$ supercomplex of maize by electron microscopy and single particle averaging gives several new insights into the architecture of these multi-protein particles. The overall L-shape of maize complex I is in agreement with previous studies on other species [1,2,7]. It strongly resembles complex I from *Arabidopsis* [12] and *Polytomella* [15]. In comparison to complex I from non-photosynthetic organisms there are two extra-domains on the membrane arm of complex I: a small intermembrane-space-exposed domain (Fig. 3, black arrows) and a larger matrix-exposed carbonic anhydrase domain (Fig. 3, white arrowheads). Careful analyses of average structures of various complex I subclasses in maize revealed the occurrence of two distinct micro-heterogeneities: (i) the length of the membrane arm was found to be 230 Å ("type I") or 215 Å ("type II"). Type II complex I at the same time exhibits an additional protrusion on the intermembrane-space side of the membrane arm opposite to the carbonic anhydrase domain (Fig. 3, white arrow); (ii) the angle between the membrane and the peripheral arm of type I complex I was either 115 or 125° (for type II complex I it always was 115°).

4.1. The maize complex I

Micro-heterogeneities of complex I particles were not reported before for plant mitochondria. In general, due to the roughness of the carbon support film on which protein molecules are absorbed during sample preparation for EM analyses, slight variations in tilting out of a stable position can happen, which might artificially lead to different projection maps. However, for reasons stated below, we rather believe that the observed structural differences are biologically significant. Three different complex I side views were observed for *Zea mays* (Fig. 3D, E, F) but only one single side view was found in *Arabidopsis* (Fig. 3L). In our interpretation the differences between the projection maps of type I (Fig. 3D) and type II complex I (Fig. 3E) point to structural differences at the tip of the membrane arm of maize complex I. The discrepancy in length cannot be sufficiently explained by tilting since the features of the hydrophilic arm and the matrix-exposed domain did not change. Notably, the length of the membrane arm in the complex I projection with the different type of handedness (Fig. 3H) is the same as in Fig. 3D and longer than the one on the type II particle of Fig. 3E. A second argument for structural variation at the tip of the *Zea mays* complex I is the fact that in *Arabidopsis* only one type of side view projection was found indicating the absence of complexes resembling *Zea mays* type II particles. Nevertheless, for the smallest differences between classes, such as the extra-domain opposite to the carbonic anhydrase domain in type II particles (white arrow, Fig. 3E), different positions on the support film cannot be excluded. To establish if this extra-domain observed in Fig. 3E is absent in the type I particles 3D information would be needed. The variation in tilt parallel to the long axis of complex I, which is probably more likely than in tilt vertical to the long axis, could be responsible as well. Such tilting could also cause the observed differences concerning the angle between the membrane and the peripheral arm of type I complex I (Fig. 3D, F). If relevant under *in vivo* conditions, the variation of the angle between the two complex I arms might reflect different complex I confirmations proposed to be important for the coupling of the electron transport and proton translocation activities of complex I [6,33].

The occurrence of complex I particles with a shorter membrane arm was observed before in NDH-1, the distantly related cyanobacterial counterpart of complex I [34]. The tip of the NDH-1 membrane arm is occupied by NdhD and NdhF subunits (the counterparts of the *Arabidopsis* mitochondrial subunits NAD4 and NAD5). There are multiple copies of the *ndhD* and *ndhF* genes, and the tip can have different compositions depending on the presence of high- and low-affinity CO_2 uptake systems [35]. In two defined particles, named NDH-1I and NDH-1M, a substantially shortened membrane arm was observed [34], probably due to the absence of NdhD and/or NdhF. The subunit composition of the plant complex I membrane arm tip is, however, not yet established.

4.2. The $I+III_2$ supercomplex

Recently, a low-resolution structure of $I+III_2$ supercomplex was solved for *Arabidopsis* [12]. At that time, no top-view

projection of complex I was available, which made the assignment of single complex I and dimeric complex III within the supercomplex less precise. After that, information of complex I in top-view position was obtained for *Polytomella* [15]. It showed that the membrane arm of complex I is not straight, but slightly bent. This bending of the complex I is also very obvious in the current I+III_2 supercomplex map from maize at 12 Å resolution (Figs. 3A, 4B) and in agreement with the recently published 8 Å projection map of complex I from *E. coli* [9]. Although some side views of complex I indicated the loss of the NADH-oxidizing unit (Fig. 3G, I), we did not observe any I+III_2 supercomplex fragments lacking this unit, as described before in *Arabidopsis* [12]. Together with the relatively high-resolution (12 Å) obtained with air-dried negatively stained specimens this indicates that the maize I+III_2 supercomplex is more stable than the one of *Arabidopsis*. The higher resolution allowed us to better assign the position of the dimeric complex III within the supercomplex by fitting of the X-ray structure (Fig. 4C, D). The complex I moiety has a good fit with the low-resolution 3D model of *Yarrowia lipolytica* [6]. The beef heart complex I particle is substantially shorter [5], as noticed earlier [12], and likely different in subunit or domain composition. In comparison to the side views of the type I and II complex I particles it appears that the complex I moiety in the I+III_2 supercomplex is composed of type I particles in maize. This would mean that the type II particles are not involved in supercomplex formation and hence could have a different function. Finally, the fitting indicates that the peripheral arm of plant complex I, which has an unknown subunit composition, has a total size and shape close to the 8-subunit *Thermus thermophilus* peripheral arm (Fig. 4A, B), despite the fact that maize and prokaryotic species are only distantly related. There is, however, a lower match at two sites. The side view map indicates that the part next to the membrane interface is positioned more to the right (Fig. 4A) and the projection map in the membrane plane indicates that the upper tip of the hydrophilic domain is wider, which could indicate additional plant subunits or domains at this position (Fig. 4B).

4.3. The carbonic anhydrase extra-domain of complex I in plants

The most characteristic feature of complex I from the C_3 plant *Arabidopsis* is the large matrix-exposed extra-domain assigned to γ-carbonic anhydrase subunits [15]. This domain also is present in the C_4 plant maize. The high-resolution of the maize complex I structure obtained by single particle averaging allowed us to compare the carbonic anhydrase domain to the X-ray structure of the prototype γ-carbonic anhydrase of the archaebacterium *Methanosarcina thermophila* [30]. Gamma-carbonic anhydrase from *M. thermophila* is homotrimeric and has a diameter of about 60 Å. The truncated X-ray structure nicely fits to the matrix-exposed extra-domain on the membrane arm of complex I

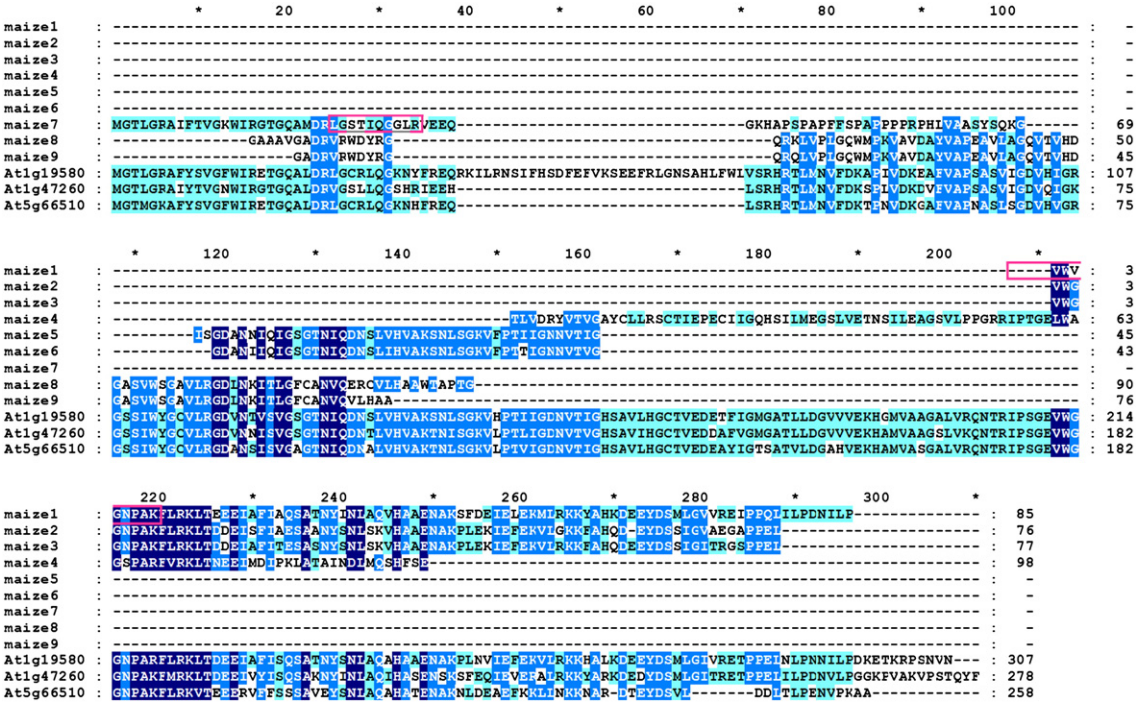

Fig. 5. Alignment of the amino acid sequences of complex I integrated carbonic anhydrases from *Arabidopsis* with putative homologues of maize. The *Arabidopsis* sequences are named according to the locus names of the *Arabidopsis thaliana* genome sequencing project at TAIR (http://www.arabidopsis.org/). Sequence At1g47260 was used as a probe to search the TIGR maize database (http://maize.tigr.org/) using the tblastn algorithm. Clones encoding nine different putative complex I integrated carbonic anhydrase subunits were identified and named "maize1" (accession: AZM4_24880), "maize2" (AZM4_51631), "maize3" (AZM4_43966), maize4 (AZM4_41212), "maize5" (AZM4_64344), "maize6" (AZM4_51632), "maize7" (AZM4_44439), "maize8" (AZM4_84283) and "maize9" (OGUBD07TV). The alignment of the sequences was carried out using clustalW at EBI (http://www.ebi.ac.uk/clustalw/) using standard parameters. Amino acids conserved in at least 7 sequences are underlayed in dark-blue, amino acids conserved in at least 6 sequences are underlayed in middle-blue and amino acids conserved in at least 3 sequences are underlayed in light-blue. The two peptide sequences identified by mass spectrometry (protein 3 in Table 1) are indicated by red boxes.

from maize (Fig. 4A). This indicates that the complex I integrated γ-carbonic anhydrase domain of *Zea mays* also is a trimer. In *Arabidopsis*, five different carbonic anhydrase subunits form part of complex I. It currently is not known whether the carbonic anhydrase domains of complex I includes three copies of the same isoform or different isoforms. Probing the maize genome sequence database (http://maize.tigr.org/) with the sequence of one of the carbonic anhydrases of *Arabidopsis* allowed to identify partial sequences of nine different putative γ-carbonic anhydrases. Since the maize genome sequence has not been completed, further homologues might exist. The two peptide sequences obtained by MS analyses of the 30 kDa subunit of maize complex I (Fig. 1, Table 1) are identical to amino acid stretches of two of the maize carbonic anhydrase isoforms (Fig. 5). Therefore, at least two forms of γ-carbonic anhydrases occur within the maize complex I. We conclude that the carbonic anhydrase domain of plant complex I most likely is heterotrimeric.

The carbonic anhydrase domain seems to be a general feature of plant complex I, since it was now described for the C_3 plant *Arabidopsis*, the C_4 plant maize and the green alga *Polytomella* [[12,15], this study]. It was proposed that the complex I integrated carbonic anhydrases might play a role in the context of a carbon transport system between mitochondria and chloroplasts to increase the efficiency of photosynthetic carbon fixation. According to this hypothesis, mitochondrial catabolism represents an important source of CO_2 for photosynthesis. The hypothesis is supported by a recent study investigating the CO_2 uptake/CO_2 fixation ratio in isolated protoplasts versus isolated chloroplasts [36]. The ratio was considerably lower in protoplasts, which was interpreted to be caused by CO_2 supply by mitochondria in protoplasts. The presence of carbonic anhydrases seems to be of equal importance in mitochondria of C_3 and C_4 plants but possibly for different reasons. In C_3 plants, CO_2 transport from mitochondria to plastids might be especially important during photorespiration, whereas in C_4 plants this transport should be most important in the context of the CO_2 liberation step in the bundle sheath cells. The CO_2 liberation step is known to be based on different enzymatic reactions, which take place in different cellular compartments [37]. In maize, the conversion of malate into pyruvate and CO_2 takes place in plastids by a $NADP^+$ dependant malic enzyme. In other plants, this step occurs in mitochondria by the act of a NAD^+ dependant malic enzyme. Alternatively, CO_2 liberation is carried out by a PEP carboxykinase localized in the cytosol of bundle sheath cells. However, the metabolism of C_4 subtypes seems not to be exclusively based on one or the other CO_2 liberation reaction, but rather on all of them to varying extends [38]. Possibly the complex I integrated carbonic anhydrases are especially important in C_4 plants with dominating NAD^+ malic enzyme dependant CO_2 liberation. Further investigations will be necessary to clarify the precise physiological role of the mitochondrial carbonic anhydrases in C_3 and C_4 plants.

Acknowledgements

We thank Dr. Roman Kouřil and Dr. Wilko Keegstra for their help with the processing and modelling of supercomplex structures and Dr. Gert Oostergetel for invaluable help with electron microscopy. We also like to thank Dr. M. Radermacher for providing *Yarrowia lipolytica* complex I images. Dagmar Lewejohann is thanked for expert technical assistance. Research of our laboratories is supported by the Deutsche Forschungsgemeinschaft (grant Br 1829-7/3).

References

[1] T. Yagi, A. Matsuno-Yagi, The proton-translocating NADH-quinone oxidoreductase in the respiratory chain: the secret unlocked, Biochemistry 42 (2003) 2266–2274.
[2] T. Friedrich, B. Böttcher, The gross structure of the respiratory complex I: a lego system, Biochim. Biophys. Acta 1608 (2004) 1–9.
[3] U. Brandt, Energy converting NADH: quinone oxidoreductase (complex I), Ann. Rev. Biochem. 75 (2006) 69–92.
[4] V. Guenebaut, R. Vincentelli, D. Mills, H. Weiss, K.R. Leonard, Three-dimensional structure of NADH-dehydrogenase from *Neurospora crassa* by electron microscopy and conical tilt reconstruction, J. Mol. Biol. 265 (1997) 409–418.
[5] N. Grigorieff, Three-dimensional structure of bovine NADH: ubiquinone oxidoreductase (complex I) at 22 Å in ice, J. Mol Biol. 277 (1998) 1033–1046.
[6] M. Radermacher, T. Ruiz, T. Clason, S. Benjamin, U. Brandt, V. Zickermann, The three-dimensional structure of complex I from *Yarrowia lipolytica*: a highly dynamic enzyme, J. Struct. Biol. 154 (2006) 269–279.
[7] L.A. Sazanov, P. Hinchliffe, Structure of the hydrophilic domain of respiratory complex I from *Thermus thermophilus*, Science 311 (2006) 1430–1436.
[8] U. Brandt, Proton-translocation by membrane-bound NADH: ubiquinone-oxidoreductase (complex I) through redox-gated ligand conduction, Biochim. Biophys. Acta 1318 (1997) 79–91.
[9] E.A. Baranova, P.J. Holt, L.A. Sazanov, Projection structure of the membrane domain of *Escherichia coli* respiratory complex I at 8 Å resolution, J. Mol. Biol. 366 (2007) 140–154.
[10] H. Schägger, K. Pfeiffer, Supercomplexes in the respiratory chains of yeast and mammalian mitochondria, EMBO J. 19 (2000) 1777–1783.
[11] H. Eubel, L. Jänsch, H.-P. Braun, New insights into the respiratory chain of plant mitochondria supercomplexes and a unique composition of complex II, Plant Physiol. 133 (2003) 274–286.
[12] N.V. Dudkina, H. Eubel, W. Keegstra, E.J. Boekema, H.-P. Braun, Structure of a mitochondrial supercomplex formed by respiratory-chain complexes I and III, Proc. Natl. Acad. Sci. U.S.A. 102 (2005) 3225–3229.
[13] J.L. Heazlewood, K.A. Howell, A.H. Millar, Mitochondrial complex I from *Arabidopsis* and rice: orthologs of mammalian and yeast components coupled to plant-specific subunits, Biochim. Biophys. Acta 1604 (2003) 159–169.
[14] P. Cardol, F. Vanrobaeys, B. Devreese, J. Van Beeumen, R. Matagne, C. Remacle, Higher plant-like subunit composition of mitochondrial complex I from: 31 conserved components among eukaryotes, Biochim. Biophys. Acta 1658 (2004) 212–224.
[15] S. Sunderhaus, N.V. Dudkina, L. Jänsch, J. Klodmann, J. Heinemeyer, M. Perales, E. Zabaleta, E.J. Boekema, H.-P. Braun, Carbonic anhydrase subunits form a matrix-exposed domain attached to the membrane arm of mitochondrial complex I in plants, J. Biol. Chem. 281 (2006) 6482–6488.
[16] L. Jänsch, V. Kruft, U.K. Schmitz, H.-P. Braun, Cytochrome *c* reductase from potato does not comprise three core proteins but contains an additional low molecular weight subunit, Eur. J. Biochem. 228 (1995) 878–885.
[17] M.J. Runswick, I.M. Fearnley, J.M. Skehel, J.E. Walker, Presence of an acyl carrier protein in NADH:ubiquinone oxidoreductase from bovine heart mitochondria, FEBS Lett. 286 (1991) 121–124.
[18] U. Sackmann, R. Zensen, D. Röhlen, U. Jahnke, H. Weiss, The acyl-carrier protein in *Neurospora crassa* mitochondria is a subunit of NADH: ubiquinone reductase (complex I), Eur. J. Biochem. 200 (1991) 463–469.
[19] E.H. Meyer, J.L. Heazlewood, A.H. Millar, Mitochondrial acyl carrier proteins in *Arabidopsis thaliana* are predominantly soluble matrix proteins and none can be confirmed as subunits of respiratory Complex I, Plant. Mol. Biol. 64 (2007) 319–327.

[20] A.H. Millar, V. Mittova, G. Kiddle, J.L. Heazlewood, C.G. Bartoli, F.L. Theodoulou, C.H. Foyer, Control of ascorbate synthesis by respiration and its implications for stress responses, Plant Physiol. 133 (2003) 443–447.
[21] G. Parisi, M. Perales, M. Fornasari, A. Colaneri, N. Schain, D. Casati, S. Zimmermann, A. Brennicke, A. Araya, J. Ferry, J. Echave, E. Zabaleta, Gamma carbonic anhydrases in plant mitochondria, Plant Mol. Biol. 55 (2004) 193–207.
[22] M. Perales, H. Eubel, J. Heinemeyer, A. Colaneri, E. Zabaleta, H.-P. Braun, Disruption of a nuclear gene encoding a mitochondrial gamma carbonic anhydrase reduces complex I and supercomplex $I+III_2$ levels and alters mitochondrial physiology in *Arabidopsis*, J. Mol. Biol. 350 (2005) 263–277.
[23] H.-P. Braun, E. Zabaleta, Carbonic anhydrase subunits of the mitochondrial NADH dehydrogenase complex (complex I) in plants, Physiol. Plant. 129 (2007) 114–122.
[24] G.D. Price, M.R. Badger, F.J. Woodger, B.M. Long, Advances in understanding the cyanobacterial CO_2-concentrating-mechanism (CCM): functional components, Ci transporters, diversity, genetic regulation and prospects for engineering into plants, J. Exp. Bot. (in press).
[25] H.-P. Braun, M. Emmermann, V. Kruft, U.K. Schmitz, Cytochrome c_1 from potato: a protein with a presequence for targeting to the mitochondrial intermembrane space, Mol. Gen. Genet. 231 (1992) 217–225.
[26] N. Hausmann, W. Werhahn, B. Huchzermeyer, H.-P. Braun, J. Papenbrock, How to document the purity of mitochondria prepared from green tissue of tobacco, pea and *Arabidopsis thaliana*, Phyton 43 (2003) 215–229.
[27] J. Heinemeyer, D. Lewejohann, H.-P. Braun, Blue-native gel electrophoresis for the characterization of protein complexes in plants, Meth. Mol. Biol. 335 (2007) 343–352.
[28] V. Neuhoff, R. Stamm, I. Pardowitz, N. Arold, W. Ehrhardt, D. Taube, Essential problems in quantification of proteins following colloidal staining with Coomassie Brilliant Blue dyes in polyacrylamide gels, and their solution, Electrophoresis 11 (1990) 101–117.
[29] M. van Heel, Similarity measures between images, Ultramicroscopy 21 (1987) 95–100.
[30] T.M. Iverson, B.E. Alber, C. Kisker, J.G. Ferry, D.C. Rees, A closer look at the active site of gamma-class carbonic anhydrases: high-resolution crystallographic studies of the carbonic anhydrase from *Methanosarcina thermophila*, Biochemistry 39 (2000) 9222–9231.
[31] S. Iwata, J.W. Lee, K. Okada, J.K. Lee, M. Iwata, B. Rasmussen, T.A. Link, S. Ramaswamy, B.K. Jap, Complete structure of the 11-subunit bovine mitochondrial cytochrome b_{c1} complex, Science 281 (1998) 64–71.
[32] N.V. Dudkina, S. Sunderhaus, H.-P. Braun, E.J. Boekema, Characterization of dimeric ATP synthase and cristae membrane ultrastructure from *Saccharomyces* and *Polytomella* mitochondria, FEBS Lett. 580 (2006) 3427–3432.
[33] B. Böttcher, D. Scheide, M. Hesterberg, L. Nagel-Steger, T. Friedrich, A novel, enzymatically active conformation of the *Escherichia coli* NADH: ubiquinone oxidoreductase (complex I), J. Biol. Chem 277 (2002) 17970–17977.
[34] A.A. Arteni, P. Zhang, N. Battchikova, T. Ogawa, E.-M. Aro, E.J. Boekema, Structural characterization of NDH-1 complexes of *Thermosynechococcus elongatus* by single particle electron microscopy, Biochim. Biophys. Acta 1757 (2006) 1469–1475.
[35] T. Ogawa, H. Mi, Cyanobacterial NADPH dehydrogenase complexes, Photosynth. Res. 93 (1–3) (2007) 69–77.
[36] K. Riazunnisa, L. Padmavathi, H. Bauwe, A.S. Raghavendra, Markedly low requirement of added CO_2 for photosynthesis by mesophyll protoplasts of pea (*Pisum sativum*): possible roles of photorespiratory CO_2 and carbonic anhydrase, Physiol. Plant. 128 (2006) 763–772.
[37] S.v. Caemmerer, R.T. Furbank, The C_4 pathway: an efficient CO_2 pump, Photosynthesis Research 77 (2003) 191–207.
[38] G.E. Edwards, R.T. Furbank, M.D. Hatch, C.B. Osmond, What does it take to be C_4? Lessons from the evolution of C_4 photosynthesis, Plant Physiol. 125 (2001) 46–49.